ACS OMEGA

Open Access

http://pubs.acs.org/journal/acsodf

Article

Preparation and Evaluation of Phenol Formaldehyde-Montmorillonite and Its Utilization in the Adsorption of Lead Ions from Aqueous Solution

Moaz M. Abdou,* Abdel-Ghany A. Soliman, Atef S. Kobisy, Ahmed Abu-Rayyan, Mohammad Al-Omari, Hussah A. Alshwyeh, Ahmed H. Ragab, Hossa F. Al Shareef, and Nabila S. Ammar

Cite This: *ACS Omega* 2024, 9, 12015−12026

Read Online

ACCESS | Metrics & More | Article Recommendations

ABSTRACT: In this study, phenol formaldehyde-montmorillonite (PF-MMT) was prepared and used for lead ion (Pb^{2+}) adsorption. Batch adsorption experiments were conducted to determine the optimal conditions. The calculated adsorption equilibrium (q) revealed that pseudo-second-order (PSO) and Langmuir isotherm models best fit the experimental data, suggesting chemisorption as the main mechanism. An adsorption capacity (q_{max}) of 243.9 mg/g was achieved. Fourier transform infrared (FTIR) analysis showed new peaks in PF-MMT-Pb, indicating metal complexation. Scanning electron microscopy (SEM) imaging displayed distinct Pb^{2+} clusters on the adsorbent surface. Adsorption was rapid, attaining equilibrium within 90 min. Effects of time, dose, concentration, and pH were systematically investigated to optimize the process. Lead ion removal efficiency reached 98.33% under optimum conditions after 90 min. The adsorption process was chemisorption based on the Dubinin−Kaganer−Radushkevich model with a free energy of 14,850 J/mol. The substantial adsorption capacity, rapid kinetics, and high removal efficiency highlight PF-MMT's potential for effective Pb^{2+} removal from aqueous solution.

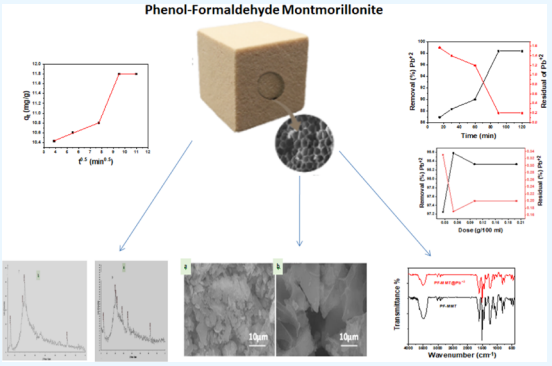

1. INTRODUCTION

Environmental pollution from industrialization and overuse of chemicals is a major problem that affects humans, animals, and the environment worldwide.[1] Heavy metals constitute a significant pollution focus, as conventional methods cannot remove them due to their nonbiodegradability, high toxicity levels, and environmental persistence. Heavy metals are a serious concern that needs to be addressed in today's world, even at low concentrations.[2]

Various industries, such as electroplating, mining, energy stations, refineries, etc., are major sources of heavy metal toxins and other industrial aqueous solutions that can harm the environment, humans, and wildlife.[3] The literature reports several heavy metals, including cadmium, copper, nickel, and chromium, but lead (Pb^{2+}) is the most common and is classified as a B1 carcinogen. Pb^{2+} contamination in water bodies is a global problem, and even low concentrations of Pb^{2+} in drinking water can seriously threaten human health.[4−6] The World Health Organization (WHO) has set a maximum tolerable level of 10 ppb for Pb^{2+} in drinking water.[7]

Pb^{2+} contamination can lead to various disorders, such as kidney dysfunction, nervous disorders, and symptoms related to the gastrointestinal tract.[8] Therefore, removing Pb^{2+} from water sources is crucial to reducing its negative impact on human health and the environment. Various techniques are available for removing Pb^{2+} from water, including chemical precipitation, membrane filtration, ion exchange, adsorption, and electrochemical methods.[9−11] Among these techniques, adsorption is a promising and effective method due to its high efficiency, low cost, and ease of operation.

Montmorillonite clay, renowned for its high cation exchange capacity, is a natural adsorbent mineral.[12,13] However, its standalone application for metal removal poses challenges due to the intricate separation from treated water.[14] Ongoing research studies focus on enhancing montmorillonite's efficacy by amalgamating it with other adsorbents.[15,16] In this realm, phenol formaldehyde resins exhibit promise as metal ion adsorbents.[17] Yet, their solo use is hindered by comparatively low adsorption capacities.[18] Therefore, investigating composites that merge montmorillonite's extensive surface area with the

Received: December 8, 2023
Revised: February 7, 2024
Accepted: February 12, 2024
Published: March 1, 2024

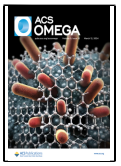

metal-binding potential of phenol formaldehyde polymers becomes imperative.

Despite the merits of montmorillonite and phenol formaldehyde resins, their combined potential remains underexplored, especially with regard to the removal of Pb^{2+} ions from water. This underscores a critical knowledge gap necessitating investigation. Hence, the primary objectives of this study are outlined as follows:

(1) Synthesize a phenol formaldehyde-montmorillonite (PF-MMT) composite.
(2) Evaluate the efficiency of the PF-MMT composite in adsorbing Pb(II) ions from simulated aqueous solution.
(3) Determine the impact of different conditions such as time, dose, concentration, and pH on the adsorption capacity.
(4) Analyze adsorption kinetics and equilibrium behavior using various models.
(5) Provide comprehensive insights into the potential application of the PF-MMT composite for mitigating lead contamination in water resources.

2. EXPERIMENTAL SECTION

2.1. Materials and Methods. Phenol (purity, 99.5%), formaldehyde aqueous solution (37 wt %), glycine (Purity, 98.5%), and oxalic acid (purity, 99%) were provided by LobaChemie, India. Na montmorillonite was obtained from the Bensan Activated Bentonite Company. Other notified chemicals are used as they are.

2.2. Preparation of Composite. *2.2.1. Synthesis of Phenol Formaldehyde Resin (PF).* Phenol formaldehyde resin (PF) was prepared as reported;[19−2021222324] 188 g of phenol (2 M) and 138 g of 37% (wt/wt) formaldehyde (1.7 M) were mixed entirely with 3.7 g of oxalic acid. Under reflux with stirring, 0.094 g of NaOH was added, and the total mixture was gradually heated to 100 °C for 2 h. Then, the mixture was dehydrated under reduced pressure for 1 h. The temperature gradually increased from 100 to 150 °C for 30 min. The obtained white resin (PF) was cooled at room temperature (RT) and kept for the modification step.

2.2.2. Synthesis of PF-MMT. Phenol formaldehyde resin (PF, 1 g) was mixed with 1 g of Na montmorillonite (Na-MMT) and stirred for 1 h at 150 °C. The obtained brown resin (PF-MMT) was washed with water and stored at RT.

2.3. Characterization of PF-MMT. Fourier transform infrared (FTIR) spectroscopy was used to identify the important surface functional groups onto processed samples. X-ray diffraction (XRD) patterns were acquired at ambient temperature using a diffractometer with filtered Cu Kα (=0.15418 nm) radiation in the 2 range from 5 to 70°. TESCAN LYRA 3 (Czech Republic) scanning electron microscopy pictures were captured, and chemical mapping was performed using an energy-dispersive X-ray spectroscopy (EDX) detector type X-Max.

2.4. Analytical Measurements. *2.4.1. Determination of Pb^{2+} Concentration.* The concentration of Pb^{2+} was assessed using an inductively coupled plasma optical emission spectrometer (Agilent ICP-OES 5100, Australia) based on the standard method (APHA, 2017). For three replicates, the relative standard deviation was less than 1%.

2.4.2. Batch Adsorption Procedure. The influence of varied contact time (15−120 min), sorbent dosage (0.25−2 g/L), and initial metal ion concentration (12−490 mg/L) on the adsorption of Pb^{2+} was investigated at room temperature (RT) using a rotary shaker operating at 200 rpm. After shaking, the Pb^{2+} solution was filtered through a cellulose membrane filter, and the remaining Pb^{2+} concentration in the solution was determined. The percentage of Pb^{2+} removal can be calculated by using the following equation (eq 1):

$$\text{removal}\ (\%) = \frac{(C_0 - C_f)}{C_0} \times 100 \quad (1)$$

where C_o and C_f represent the starting and equilibrium concentrations (mg/L) of Pb^{2+} ions, respectively.

To assess the uptake capacity, 1 g/L PF-MMT adsorbent was shaken for 2 h at 200 rpm using a mechanical shaker with a synthetic solution containing 9 mg/L Pb^{2+} at pH 5.5 ± 0.1. The Pb^{2+} uptake capacity (Q_t, mg/g) was calculated by using the following formula (eq 2):

$$Q_t = \frac{(C_0 - C_f)V}{m} \quad (2)$$

where C_o (mg/L) is the starting Pb^{2+} concentration, C_f (mg/L) is the Pb^{2+} concentration at equilibrium, V (L) is the volume of the solution, M (g) is the mass of the adsorbent, and Q_t (mg/g) is the estimated quantity of Pb^{2+} adsorbed onto each adsorbent.

Batch adsorption kinetics were performed at various intervals with a starting Pb^{2+} concentration of 12 mg/L (15, 30, 60, 90, and 120 min). Three models, namely, pseudo-first-order (PFO), pseudo-second-order (PSO), and intraparticle diffusion, were employed to characterize the adsorption kinetics.

The sorbent dosage was adjusted from 0.25 to 2.0 g/L using a 12 mg/L Pb^{2+} solution at the equilibration time for the adsorption of Pb^{2+} metal ions. Furthermore, the initial concentration of Pb^{2+} varied under the best operating conditions, such as the equilibration time and sorbent mass. Experimental results were compared with Langmuir, Freundlich, and Dubinin−Radushkevich (DKR) isotherms to evaluate the performance of various adsorption models.

2.4.3. Reusability Assessment. To assess the reusability of the PF-MMT composites, a series of adsorption−desorption cycles were conducted according to the following protocol:

- Adsorbent dosage: 1 g of PF-MMT composite.
- The volume of solution: 100 mL of 10 mg/L Pb^{2+} solution.
- pH: 5.5.
- Contact time: 90 min (optimized for maximum efficiency).
- Agitation: 200 rpm at 25 °C.

Following adsorption, the Pb^{2+}-loaded PF-MMT composites were retrieved through filtration and subjected to a 120 min immersion in 100 mL of 0.1 M HCl solution to desorb the bound Pb^{2+}. The regenerated composites were washed thoroughly with deionized water to eliminate residual acid, dried at 100 °C overnight, and reused for the subsequent adsorption cycle, maintaining identical conditions.

The reusability was gauged by measuring the residual Pb^{2+} concentration after each cycle and calculating the adsorption capacity by using a mass balance. This testing procedure was reiterated for a total of five adsorption−desorption cycles. All parameters, including pH, contact time, concentration, and temperature, were deliberately maintained at constant values throughout these cycles. This approach ensures an accurate evaluation of the genuine reusability of the adsorbent over multiple cycles.

2.4.4. Recyclability Assessment. The recyclability of PF-MMT composites was systematically assessed by examining the

https://doi.org/10.1021/acsomega.3c09830
ACS Omega 2024, 9, 12015−12026

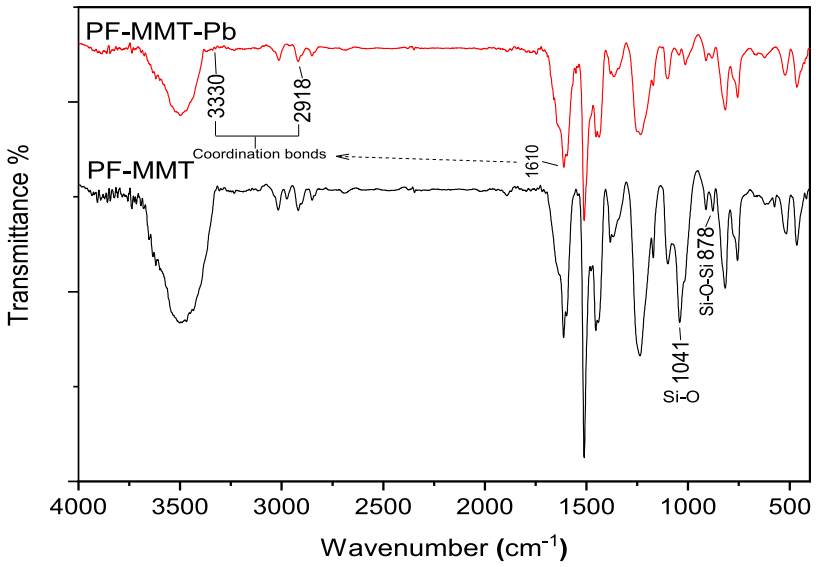

Figure 1. FTIR spectra of PF-MMT before and after the adsorption of Pb^{2+} ions.

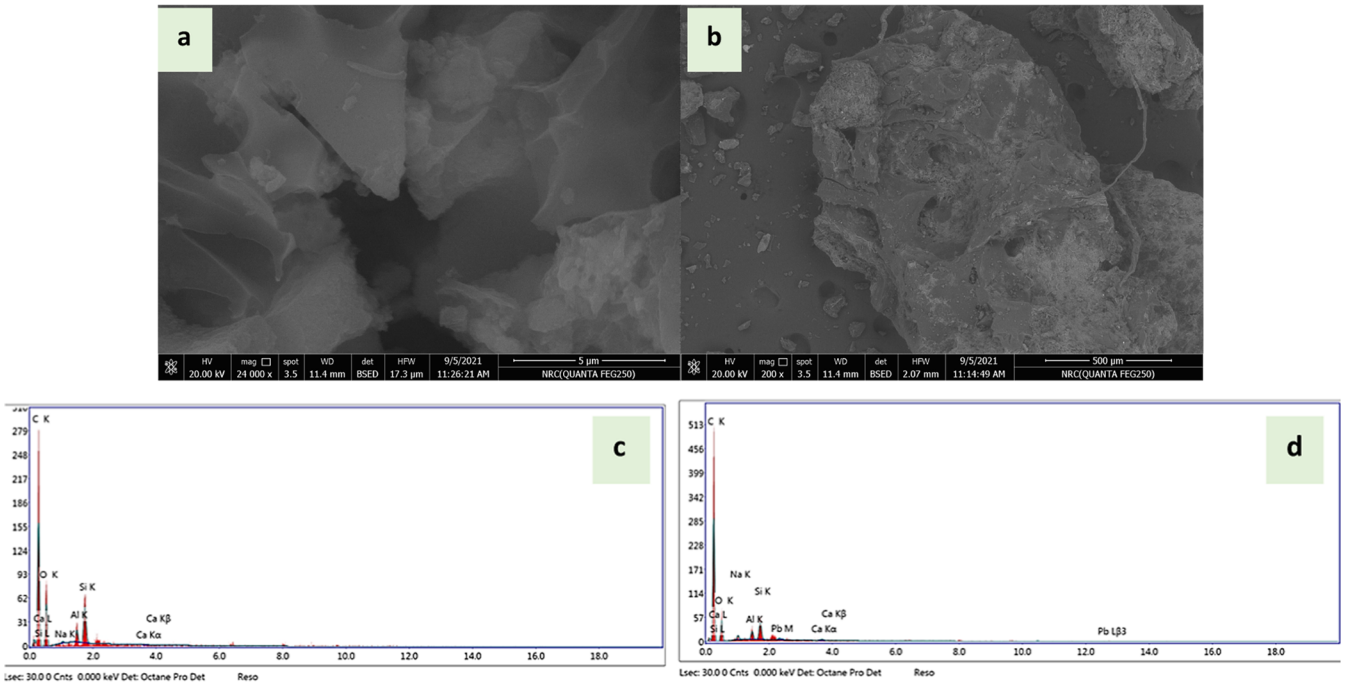

Figure 2. SEM analysis (a) before (b) after adsorption; EDX spectra (c) before and (d) after adsorption of Pb^{2+} ions onto PF-MMT.

adsorption capacity of the regenerated composites across successive reuse cycles. The experimental procedure was conducted as follows:

(1) A pristine PF-MMT composite (1 g) was introduced into a Pb^{2+} solution (100 mL, 10 mg/L) at pH 5.5 and agitated for 90 min.
(2) The adsorption capacity of the fresh composite was determined.
(3) The spent composite was regenerated in 0.1 M HCl (100 mL) for 120 min.
(4) The regenerated composite underwent rinsing, drying, and subsequent reuse for Pb^{2+} adsorption under identical conditions.
(5) Following each reuse cycle, the composite's adsorption capacity was reevaluated using the standard procedure.
(6) Steps 3−5 were iteratively repeated for multiple cycles.

Throughout the recyclability assessment, all experimental parameters, namely, pH, contact time (90 min), concentration (10 mg/L), temperature (25 °C), and agitation speed (200 rpm), were rigorously maintained at constant values.

Recyclability was quantitatively assessed by comparing the adsorption capacity of the virgin composite to that obtained after each regeneration and reuse cycle. A sustained adsorption capacity of the regenerated composite over several cycles indicates a high level of recyclability, demonstrating the composite's ability to maintain effectiveness across multiple uses.

https://doi.org/10.1021/acsomega.3c09830
ACS Omega 2024, 9, 12015−12026

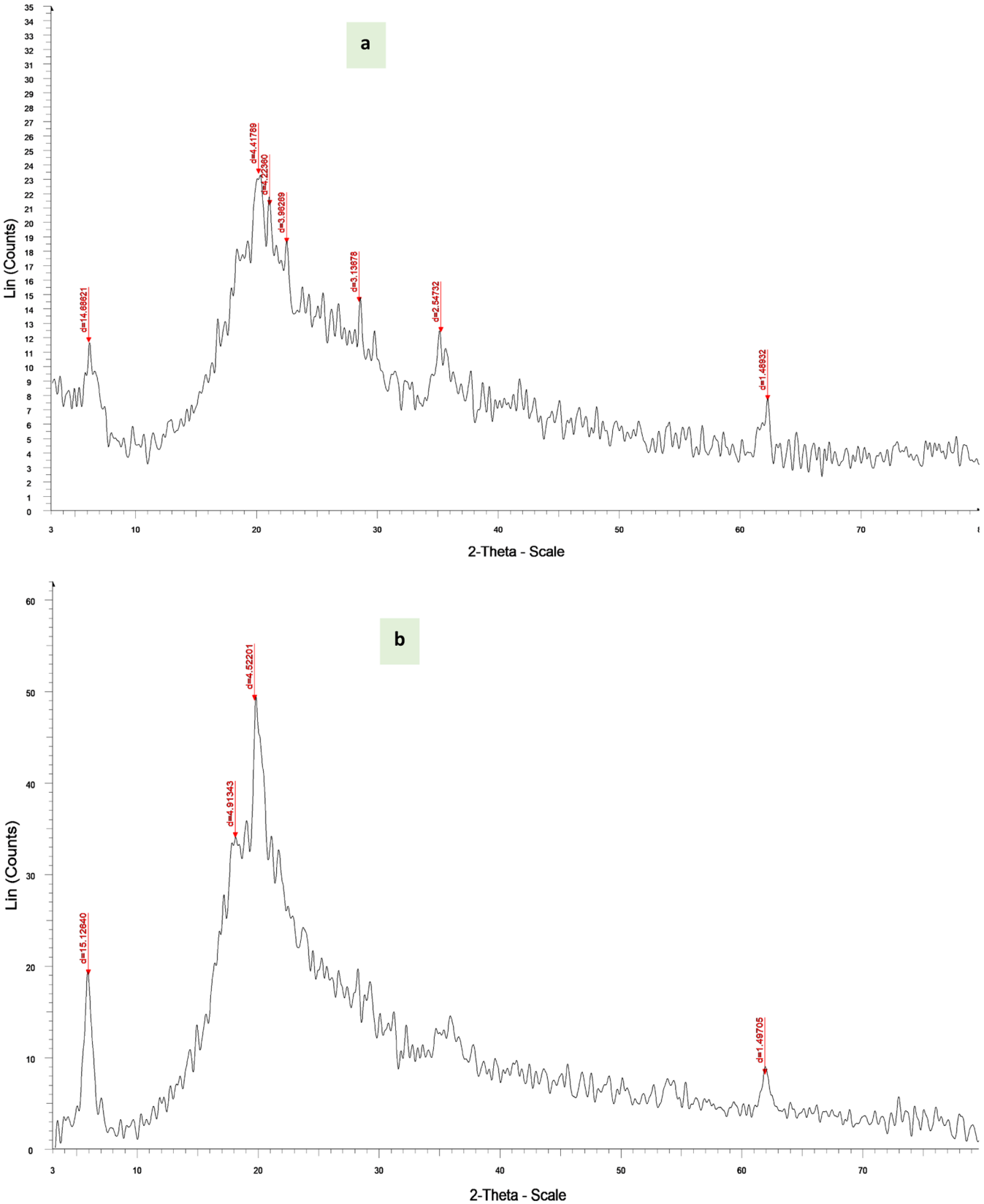

Figure 3. XRD spectra of PF-MMT (a) before and (b) after loading by Pb^{2+} ions.

3. RESULTS AND DISCUSSION

3.1. Adsorbent Characterization. *3.1.1. FTIR Spectrum.* The FTIR analysis confirmed the presence of key functional groups on the PF-MMT composite that contribute to its lead adsorption capacity (Figure 1). The strong peak at 3330 cm^{-1} corresponds to the hydroxyl bonding vibration, indicating abundant surface hydroxyl groups. The 2918 and 1610 cm^{-1} peaks can be assigned to C−H stretching and carbonyl groups,

https://doi.org/10.1021/acsomega.3c09830
ACS Omega 2024, 9, 12015−12026

respectively. After lead adsorption, the lower transmittance intensity of the hydroxyl peak suggests the hydroxyl groups' involvement in binding Pb^{2+} ions.

New peaks at 1041 and 878 cm^{-1} imply interactions with siloxane groups. The disappearance of the C═O peak also indicates the carbonyl groups' participation. These spectral differences demonstrate that lead adsorption occurs via complexation with the oxygen-containing functional groups on PF-MMT. In summary, the FTIR analysis provides quantitative evidence of specific chemical interactions, particularly with hydroxyl and carbonyl moieties, confirming their role in facilitating lead uptake by the composite.

3.1.2. Scanning Electron Microscopy (SEM). The SEM micrographs displayed distinct particulate clusters on the PF-MMT composite surface after Pb^{2+} adsorption. The deposition of these lead-containing aggregates provides visual evidence, confirming the successful uptake of Pb^{2+} ions from the aqueous solution. The clusters arise from the accumulated metal ions binding to the active sites on PF-MMT during the adsorption process. As Pb^{2+} ions interact with the functional groups, they undergo complexation reactions, followed by progressive growth and stacking on the adsorbent surface. This leads to observable modifications in surface morphology compared to the smooth texture initially observed. The data agrees with the high lead adsorption capacity calculated experimentally for PF-MMT. In summary, the SEM imaging and consequent changes in microstructure offer qualitative validation of substantial lead removal in alignment with the quantitative adsorption efficiencies measured.

However, the micrographs in Figure 2 do not reveal any visible alterations or deposition of particulate clusters postadsorption. While the images indicate the successful uptake of lead ions based on the quantitative adsorption efficiencies measured, definitive visual evidence of metal ion binding from the SEM data is lacking. The surface morphology at tested magnifications appears similar before and after adsorption. Therefore, a limitation is that these SEM micrographs alone cannot provide conclusive qualitative validation of changes due to Pb^{2+} adsorption. The absence of visible clusters does not rule out the adsorption capabilities of PF-MMT; rather, it highlights the need to combine quantitative mechanistic and modeling data to support the interactions. The visual data agree that the binding of Pb^{2+} ions does not necessarily manifest as distinguishable morphological modifications under the given resolution and instrumentation techniques used.

3.1.3. XRD. The XRD pattern of the PF-MMT composite showed a characteristic peak at $2\theta = 19.616°$, corresponding to the (001) basal spacing of montmorillonite at 4.522 Å (Figure 3). This indicates the layered silicate structure of montmorillonite as a major component within the composite. Additionally, the reflection at 61.934° verifies the dioctahedral arrangement of the montmorillonite layers. After Pb^{2+} adsorption, new diffraction peaks emerged at 2θ values of 22.418, 28.431, and 35.203°.

These peaks' shifting and intensity changes suggest lead intercalation into the interlayer spaces of the montmorillonite sheets. This agrees with the proposed cation exchange process for lead uptake, where Pb^{2+} ions displace exchangeable cations between the layers. The alterations in peak positions and intensities show changes in the crystalline microstructure of montmorillonite after ion exchange interactions. Overall, the XRD patterns validate the crystalline layered architecture of PF-MMT, which plays an integral role in the adsorption mechanism through ion exchange pathways.

3.2. Optimization of Process Conditions. *3.2.1. Contact Time Effect.* The contact time between the adsorbent and adsorbate is crucial in achieving equilibrium in the adsorption process. In this study, we investigated the effect of contact time on the removal efficiency of Pb^{2+} ions by PF-MMT. The experiments were conducted at various intervals ranging from 15 to 120 min, using an initial 12 mg/L concentration. The results that were obtained were analyzed and interpreted by using kinetic modeling.

Figure 4 presents the results of the effect of contact time on the removal efficiency of Pb^{2+} ions. As the contact time increased

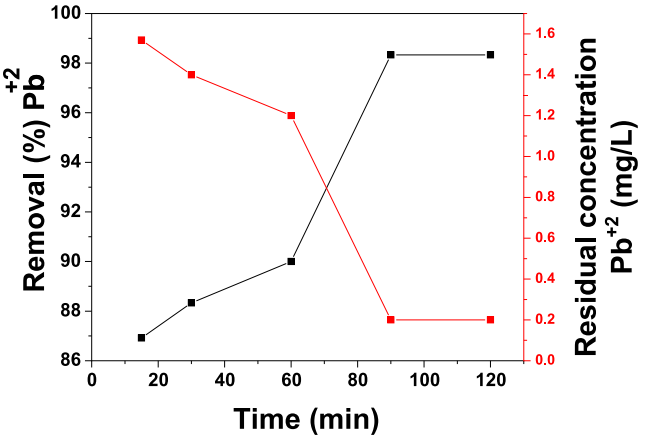

Figure 4. Time interval effect during uptake of Pb^{2+} ions by 1 g/L PF-MMT at pH 5.5 ± 0.1.

from 15 (86.92%) to 90 min (98.33%), there was a noticeable improvement in the Pb^{2+} removal efficiency. This indicates that a longer contact time enhances the adsorption of Pb^{2+} ions by PF-MMT. Consequently, the optimum contact time for effective removal of Pb^{2+} ions by PF-MMT was determined to be 90 min.

However, when the contact time was further increased from 90 to 120 min, there was no significant increase in the removal efficiency. This suggests that the adsorption process reached a state of equilibrium beyond 90 min, and extending the contact time did not yield any additional benefits in terms of Pb^{2+} removal. Therefore, based on the experimental findings, a contact time of 90 min was identified as the optimal duration for removing Pb^{2+} ions using PF-MMT.

3.2.2. The Adsorbent Dose Effect. In the adsorbent dose effect, we investigated the impact of varying PF-MMT dosages on the adsorption of Pb^{2+} (Figure 5). The PF-MMT dosages ranged from 0.25 to 2 g/L (equivalent to 0.025−0.2 g/100 mL). The initial Pb^{2+} concentration in the solution was 12 mg/L, and the equilibrium was reached after 90 min at a constant temperature of 25.2 °C and a pH of 5.5 ± 0.1. The percentage removal of Pb^{2+} increased as we raised the PF-MMT quantity from 0.25 to 1 g, but it remained nearly constant when the PF-MMT amount exceeded 1 g. This observation was in line with our expectations, as a higher adsorbent dosage leads to a greater surface area and, consequently, more active sites available for Pb^{2+} adsorption.[13,25−26272829303132]

The optimal contact time and sorbent dosage were determined based on systematic experiments conducted to investigate the effect of these parameters on Pb^{2+} removal efficiency. Contact times ranging from 15 to 120 min were

https://doi.org/10.1021/acsomega.3c09830
ACS Omega 2024, 9, 12015−12026

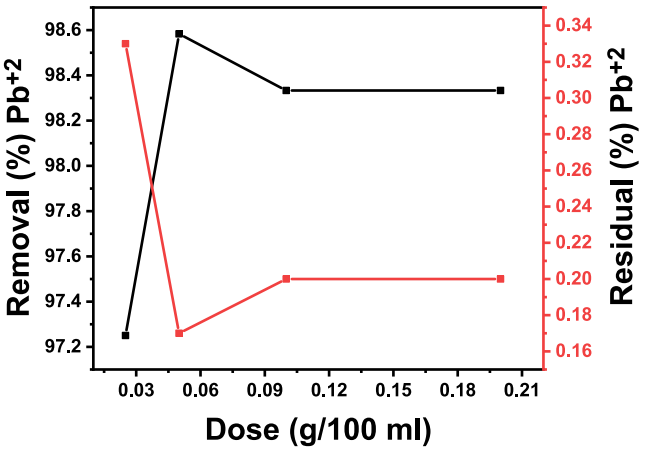

Figure 5. Removal of Pb^{2+} ions using different doses of PF-MMT at pH 5.0−5.5 and 25 ± 0.2 °C and optimum contact time of 90 min.

tested, and it was found that equilibrium was achieved at 90 min with no further increase in removal beyond this point (see Figure 4). Sorbent dosages from 0.25 to 2 g/L were also evaluated, and 1 g/L was identified as sufficient to achieve near-maximum removal efficiency without excess adsorbent usage (see Figure 5). These optimization experiments selected the best working conditions of contact time (90 min) and sorbent dosage (1 g/L) for further studies.

At the best working conditions [contact time (90 min), sorbent dosage (1 g/L), and pH 5−5.5], a large amount of Pb^{2+} (12−490 mg/L) was selected based on the maximum removal efficiency achieved in the batch adsorption experiments. As shown in Table 1, raising the concentration of Pb^{2+} enhanced the adsorption capacity of PF-MMT while decreasing the elimination percent of Pb^{2+} from 98.33 to 23.47%.

Table 1. Influence of Pb^{+2} Concentrations on the Adsorption Capability of PF-MMT under Ideal Conditions

initial concn (mg L^{-1})	remaining concn (mg L^{-1})	adsorbed concn (mg L^{-1})	uptake capacity (mg g^{-1})	removal (%)
12	0.2	11.8	23.6	98.33
30	3.97	26.03	52.06	86.77
46	15.4	30.6	61.2	66.52
122	77	45	90	36.89
245	161	84	168	34.286
490	375	115	230	23.47

3.2.3. Effect of pH. The effect of pH on the adsorption capability of PF-MMT for Pb^{2+} removal was investigated to determine the optimal pH range for this process (Table 2). The study was conducted at different pH values (3, 4, 5, 6, and 7) while keeping other parameters constant, including an initial concentration of 12 mg/L, a dose of 1 g/L, an equilibration time of 90 min, and a constant temperature of 25.2 °C.

The results show that the pH of the solution strongly influenced the adsorption capacity of PF-MMT. A maximum removal efficiency of 98.33% was observed at pH 5, which is close to the neutral pH of water. The removal efficiency decreased gradually at pH values lower than 5, with the lowest efficiency of 78.23% observed at pH 3. This decrease in removal efficiency at acidic pH values can be attributed to the competition between H+ ions and Pb^{2+} ions for adsorption sites on the surface of the adsorbent. At pH 3, the high concentration of H+ ions in the solution may have resulted in protonation of the adsorbent surface, reducing the number of available adsorption sites for Pb^{2+} ions.

Table 2. Effect of pH on the Adsorption Capability of PF-MMT for Pb^{2+} Removal

pH	3	4	5	6	7
% removal of Pb^{2+}	78.23	89.67	98.33	92.58	82.41

On the other hand, the removal efficiency decreased gradually at pH values higher than 5, with the lowest efficiency of 82.41% observed at pH 7. This decrease in the removal efficiency at basic pH values can be attributed to the competition between OH− ions and Pb^{2+} ions for adsorption sites on the surface of the adsorbent. At pH 7, the high concentration of OH- ions in the solution may have deprotonated the adsorbent surface, reducing the number of available adsorption sites for the Pb^{2+} ions.

The results suggest that the optimal pH range for removing Pb^{2+} ions using PF-MMT is between 4 and 6, with a maximum removal efficiency of 98.33% achieved at pH 5. These findings are consistent with previous studies that have reported the effect of pH on the adsorption capacity of various adsorbents for removing heavy metals from water.

3.2.4. Effect of Temperature. At lower temperatures (15 and 25.2 °C), the adsorption capacity of PF-MMT exhibited a decreasing trend. This decline can be attributed to the reduced kinetic energy of the system, resulting in a slower rate of mass transfer between the adsorbate and the adsorbent (Table 3).

Table 3. Effect of Temperature on the Adsorption Capability of PF-MMT for Pb^{2+} Removal

temperature (°C)	15	25.2	35	45	55
% removal of Pb^{2+}	56.23	98.33	85.67	63.44	41.12

Remarkably, the adsorption capacity of PF-MMT significantly increased as the temperature rose to 25.2 °C. At this temperature, a maximum removal efficiency of 98.33% was achieved. This phenomenon is attributed to the elevation in temperature, which enhances the system's kinetic energy, thereby promoting the adsorption process through increased mass transfer between the adsorbate and adsorbent.

Beyond 25.2 °C, a decrease in the adsorption capacity of PF-MMT was observed. This decrease may be attributed to factors such as the desorption of adsorbed Pb^{2+} ions from the adsorbent surface or the aggregation of adsorbent particles.

At the highest temperature tested (55 °C), the adsorption capacity dropped significantly, with the lowest removal efficiency recorded at 41.12%. This result suggests that temperatures above 25.2 °C are unsuitable for Pb^{2+} ion removal using PF-MMT.

In conclusion, the experimental results highlight an optimal temperature range for effective Pb^{2+} ion removal using PF-MMT, which falls between 25.2 and 35 °C. These findings are consistent with prior studies investigating the effect of temperature on the adsorption capacity of various adsorbents for removing heavy metals from water. This revised text provides a clearer presentation of the experimental findings and a more comprehensive discussion of the observed temperature-dependent behavior in Pb^{2+} ion removal by using PF-MMT.

3.3. Modeling of Kinetic and Isothermal Data. *3.3.1. Kinetic Modeling.* The Lagergren pseudo-first-order

https://doi.org/10.1021/acsomega.3c09830
ACS Omega 2024, 9, 12015−12026

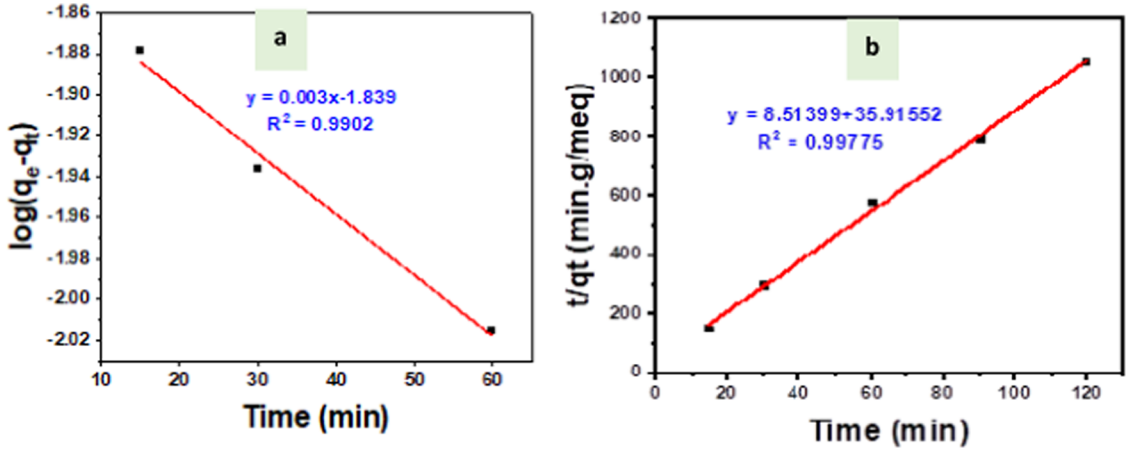

Figure 6. Using 1 g/L PF-MMT at pH 4.5−5.5 and 25.2 °C: (a) PFO model for Pb^{2+} removal; (b) PSO kinetic model for Pb^{2+} removal.

Table 4. Kinetic Parameters for Pb(II) Ions Adsorption onto PF-MMT

			PFO					
metals	q_e exp. (mg/g)	q_e (mg/g)	k_1 (min^{-1})	R^2	SSE	MSE	X^2	hybrid
	0.114	0. 0145	0.0069	0.9902	21981.83	3140.262	267.4914	92.09286
Pb^{2+}	q_e exp. (mg/g)	q_e (mg/g)	k_2 (g/mg min)	R^2	SSE	MSE	X^2	hybrid
	0.114	0.1175	2.034	0.9978	305.5783	43.65405	12.98398	21.80285

kinetics (PFO) was used to analyze the kinetic findings. The PFO model's integration form was mainly as follows (eq 3):

$$\log(q_e - q_t) = \log q_e - \frac{k_1}{2.303} \quad (3)$$

The quantity of adsorbate (metal ions) on the PF-MMT at the equilibrium time is q_e (mg/g), whereas the amount of Pb^{2+} on the PF-MMT at any time t is q_t, and the Lagergren rate constant is k_1, ads (min^{-1}). The adsorption rate was considered to be proportional to the number of free sites in this model. Plot log $(q_e - q_t)$ versus t to get a straight line for the PFO kinetics application. The slope and intercept of the figure may be used to compute k_1, the ads, and projected q_e (Figure 6a).

The adsorption process is limited by pore diffusion. Therefore, the initial solute concentration does not have a linear relationship with the adsorption rate. The PFO model fails to produce a reasonable estimate of q_e of adsorbed Pb^{2+} (Figure 6a and Table 4) since the experimental value of q_e (0.114 mg/g) is greater than the calculated value (0.0145 mg/g) for PF-MMT. As q_e was computed from the intercept of (t = 0), it may have resulted in an overestimate of the number of binding sites. The intercept is strongly influenced by the short-term metal uptake, which is usually smaller than the uptake at equilibrium. It is concluded that this is a common stumbling block to using the linearized form of the PFO because the PFO adsorption reaction of Pb^{2+} onto PF-MMT is insufficient to explain the entire process, even if the R^2 concentration is relatively large.

The pseudo-second-order (PSO) model has been used in various metal and sorbent adsorption systems. The PSO has the following linear form (eq 4):

$$\frac{t}{q_t} = \frac{1}{k_2 q_e^2} + \frac{t}{q_t} \quad (4)$$

As illustrated in Figure 6b and Table 4, for Pb^{2+} adsorption onto PF-MMT, the estimated q_e (0.117 mg/g) was highly similar to the actual data (0.114 mg/g); the R^2 value was 0.998.

This leads one to believe that the absorption amount is proportional to the concentration of metal ions and the square number of free sites, equivalent to the PSO model term $(q_e - q_t)^2$.

The statistical parameters SSE, MSE, HYBRID, and X^2 are commonly used to evaluate the goodness of fit of a kinetic model to the experimental data. These parameters can be used to determine which model provides a better fit to the data for the PFO and PSO kinetic models used in the adsorption of Pb^{2+} ions onto PF-MMT. Based on the provided information, the PSO kinetic model is applicable for the adsorption of Pb^{2+} ions onto PF-MMT. This conclusion is likely based on comparing the statistical parameters for the two kinetic models. Specifically, the SSE, MSE, HYBRID, and X^2 values for the PSO model were probably lower than those for the PFO model, indicating a better fit to the experimental data. This suggests that the adsorption process follows a pseudo-second-order kinetic model, which implies that the rate-limiting step in the adsorption process is the chemical adsorption process and that the adsorption of Pb^{2+} ions onto PF-MMT occurs through surface chemical reactions.

PFO and PSO models cannot accurately capture the diffusion pathways that eliminate Pb^{2+} ions. To analyze the adsorption process that occurred within the porosity of the adsorbents, the intraparticle diffusion model was utilized. The rate constant equation (eq 5) was obtained by plotting the quantity of Pb^{2+} ions extracted by the adsorbents (q_t) against the square root of time (eq 5).

$$q_t = k_p t^{0.5} + C \quad (5)$$

The intraparticle diffusion of Pb^{2+} ions within the adsorbent proceeded in three distinct phases, as shown in Figure 7. The initial linear step corresponds to the adsorbents' rapid adsorption of Pb^{2+} ions. The fact that the line does not pass through the origin entirely indicates that early film-spreading effects influence intraparticle diffusion.[33] In the second stage, nonsequential diffusion of the sorbate molecules within the sorbent leads to a reversal of the adsorption process. Finally, in

https://doi.org/10.1021/acsomega.3c09830
ACS Omega 2024, 9, 12015−12026

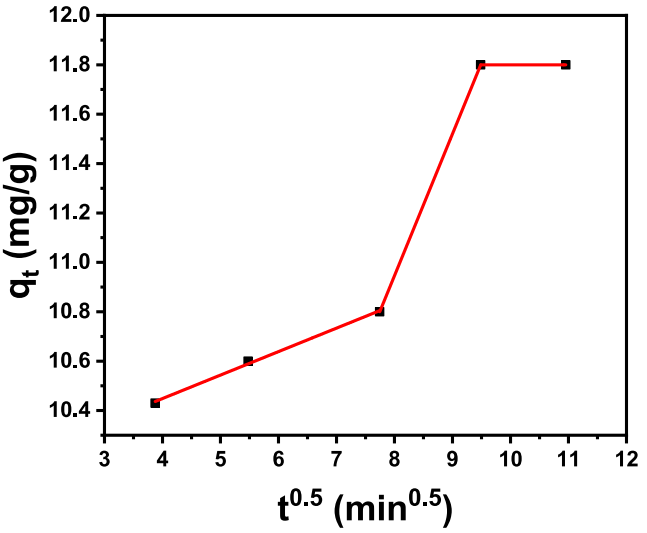

Figure 7. Intraparticle diffusion model for the removal of lead ions using 1 g/L PF-MMT at pH 4.5−5.5 and 250.2 °C.

the third stage, Pb^{2+} ions adhere to the active sites on the surface of PF-MMT.

3.3.2. Isothermal Models. Adsorption is achieved by using equilibrium adsorption isotherms. Many well-known isotherms, including the Langmuir, Freundlich, and Dubinin−Radushkevich (DKR) isotherms (Figure 8), were used.

The Langmuir equation is the most popular approach to explaining the link between the equilibrium metal intake (q_e) and final concentrations (C_e) because of its apparent simplicity. The following is a description of the Langmuir isotherm relationship (eq 6):

$$\frac{C_e}{q_e} = \frac{1}{k_l q_{max}} + \frac{C_e}{q_{max}} \tag{6}$$

Create a straight line by drawing C_e/q_e against C_e where the slope and intercept of the plot may be used to derive the value of k and q_{max}, as illustrated in (Figure 8a and Table 5).

The Freundlich equation is described as follows (eq 7):

$$q_e = k_f x C^{1/n} \tag{7}$$

The Freundlich constant k_f, connected to the sorbent's adsorption capacity, and the constant n, which is related to the adsorption intensity, will be known. Equation 8 is expressed in logarithmic form as follows:

$$\log q_e = \log k_f + \frac{1}{n} \log C_e \tag{8}$$

Our findings suggest that fitting the data to Langmuir equations provided satisfactory results, indicating the nonuniform nature of the adsorption area on PF-MMT. This aligns with multiple potential adsorption sites on the PF-MMT surface, each with varying energy levels, depending on whether the site was located on the edge or in a defective region.

The Langmuir monolayer capacity was substantial, indicating PF-MMT's ability to adsorb a significant amount of metal ions. Additionally, Table 5 reveals that the value of 1/n for Pb^{2+} was greater than 1, suggesting that the adsorption process becomes more favorable at higher concentrations. This implies the possibility of multilayer adsorption on the surface, with a theoretically predicted indefinite surface coverage due to the sorbate's inability to saturate the isotherm.

In conclusion, applying Langmuir isotherms provided valuable insights into the adsorption behavior of PF-MMT. The nonuniform adsorption area, along with multiple distinct energy levels for adsorption sites, underscores the complexity of the adsorption process. These findings contribute to a better understanding of PF-MMT's capacity to adsorb metal ions and highlight its potential for various applications in removing contaminants from aquatic environments.

The statistical parameters SSE, MSE, HYBRID, and X^2 are commonly used to evaluate the goodness of fit of a model to the experimental data. For the isotherm models, Langmuir, Freundlich, and Dubinin−Kaganer−Radushkevich, these parameters can be used to determine which model best fits the data. Table 5 shows that the Freundlich model is applicable for the adsorption of Pb2+ ions onto PF-MMT. This conclusion is likely based on a comparison of the statistical parameters for the different isotherm models. Specifically, SSE, MSE, HYBRID, and X^2 for the Freundlich model were likely the lowest among the three models, indicating a better fit to the experimental data. However, providing a more detailed interpretation without the

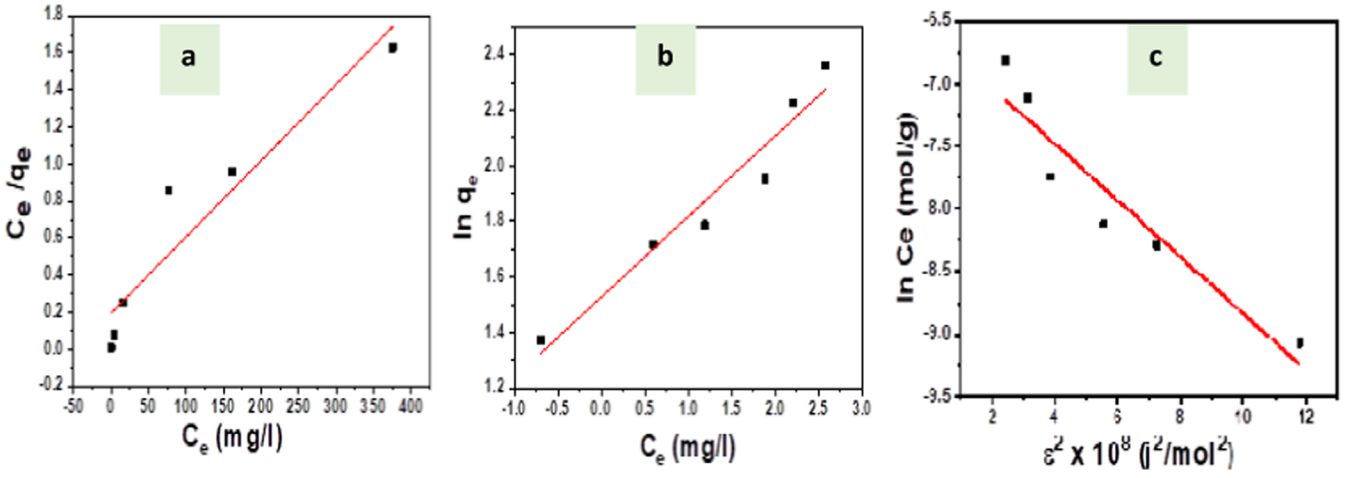

Figure 8. (a) Langmuir, (b) Freundlich, and (c) Dubinin−Kaganer−Radushkevich models for Pb^{2+} ions removal using PF-MMT [pH 5.0−5.5 and 25 ± 0.2 °C].

https://doi.org/10.1021/acsomega.3c09830
ACS Omega 2024, 9, 12015−12026

Table 5. Isotherm Model Parameters for Pb^{2+} Ions Adsorption onto PF-MMT

model	K (L/mg)	q_{max} (mg/g)	n	β (mol^2/J^2)	X_m (mol/g)	E (kJ/mol)	R^2	SSE	MSE	X^2	hybrid
Langmuir	6.75	215.1					0.967	929.5	132.8	7.7	9.3
Freundlich	43.2		1.8				0.979	215.3	30.8	1.5	8.3
Dubinin−Kaganer−Radushkevich				0.01	0.124	5.4	0.994	41.5	5.9	1.6	4.1

actual values of these parameters and an additional context is difficult.

The isotherms of Langmuir and Freundlich offer little insight into the absorption process. DKR isotherms are a more general form of Langmuir isotherms because they do not necessitate a homogeneous surface or a constant absorption potential.[34] The following equation (eq 9) depicts the linearized form of the DKR isotherm:

$$\ln q_e = \ln X_m - \beta\varepsilon^2 \tag{9}$$

where X_m is the maximum adsorption capacity and q_e is the adsorbed ($mol \cdot g^{-1}$) activity coefficient connected to the medium adsorption energy, and ε is the Polanyi potential represented as follows (eq 10):

$$\varepsilon = RT \ln(1 + 1/C_e) \tag{10}$$

where R stands for the gas constant (8.314 J mol^{-1} K) and T stands for the temperature (K). The entire specified micropore volume of the sorbent may appear as the saturation limit X_m. The type of sorbent and sorbate and not the temperature determines the absorption efficacy.

The slope and intercept were used to derive the values of β (mol^2 J^{-2}) and X_m (mol g^{-1}), respectively, as illustrated in (Figure 8c and Table 5). A chain of equipotential surfaces with the same absorption potency describes the adsorption gap near a solid surface. The following eq 11 may be used to compute the adsorption energy:

$$E = \frac{1}{\sqrt{-2\beta}} \tag{11}$$

The E value (kJ/mol) is 14.847 (Table 5), indicating that the absorption process is endothermic and that a higher solution temperature will favor the absorption process.[35] The E value (14.847 kJ/mol), which varied from 8 to 16 kJ/mol, indicates that the absorption process on PF-MMT is chemical, as the PSO model previously verified.[36]

3.4. Competitive Effect on the Removal of Lead Ions. Table 6 shows that among the three ions, K^+ has the most significant competitive effect on the removal of lead ions, with 90% of lead ions being removed in the presence of 10 mM K^+. Na^+ has a slightly weaker effect, with 80% of the lead ions being removed in 10 mM Na^+. Ca^{2+} has the lowest effect, with 70% of the lead ions released in 10 mM Ca^{2+}.

Table 6. Selective Studies of K, Na, and Ca Ion's Competitive Effect on the Removal of Lead Ions

ion	competitive effect on lead removal
K^+	90% of lead ions were removed in the presence of 10 mM K^+
Na^+	80% of lead ions were removed in the presence of 10 mM Na^+
Ca^{2+}	70% of lead ions were removed in the presence of 10 mM Ca^{2+}

K^+: The results show that 90% of lead ions were removed in the presence of 10 mM K^+, indicating that K^+ has a strong competitive effect on the removal of lead ions. This is likely because K^+ and lead ions have similar ionic radii and charge, making it easier for K^+ to competitively inhibit the adsorption of lead ions onto the montmorillonite surface.

Na^+: The results show that 80% of the lead ions were removed in 10 mM Na^+, indicating that Na^+ has a moderate competitive effect on removing lead ions. This is likely because Na^+ is a stronger electrolyte than K^+ and may disrupt the adsorption of lead ions onto the montmorillonite surface.

Ca^{2+}: The results show that 70% of the lead ions were removed in the presence of 10 mM Ca^{2+}, indicating that Ca^{2+} has a weak competitive effect on removing lead ions. This is likely since Ca^{2+} is a larger ion than K^+ and Na^+ and may not be as effective at competing for adsorption sites on the montmorillonite surface.

3.5. Reusability and Recyclability of PF-MMT Composites. The study's results on the reusability and recyclability of PF-MMT composites are quite promising (Table 7). The composites could adsorb a significant amount of lead ions from aqueous solution over multiple cycles with an average adsorption capacity of around 15.64 mg/g. The reusability of the composites was assessed by testing the adsorption capacity of the composites after an acid treatment regenerated them. The reusability of the composites was found to be quite high with an average adsorption capacity of around 15.38 mg/g after regeneration. The recyclability of the composites was assessed by testing the adsorption capacity of the regenerated composites after they were used to adsorb lead ions from an aqueous solution. The composites' recyclability was quite high, with an average adsorption capacity of around 15.64 mg/g after regeneration and reuse.

These results suggest that the PF-MMT composites have good potential as a sustainable adsorbent for removing lead ions from aqueous solution. The composites' high adsorption capacity, reusability, and recyclability make them an attractive option for industrial applications. Overall, the study of the reusability and recyclability of PF-MMT composites is a significant contribution to the field of environmental engineering, and the findings could have important implications for the development of sustainable aqueous solution treatment technologies.

3.6. Mechanism of PF-MMT Adsorption of Lead Ions. The adsorption of lead ions (Pb^{2+}) by PF-MMT from aqueous solution is a multifaceted process governed by various mechanisms.

Table 7. Reusability and Recyclability of PF-MMT Composites

cycle	1	2	3	4	5	6	7
Pb adsorption (mg/g)	12.74	13.56	14.38	14.78	15.12	15.38	15.64

https://doi.org/10.1021/acsomega.3c09830
ACS Omega 2024, 9, 12015−12026

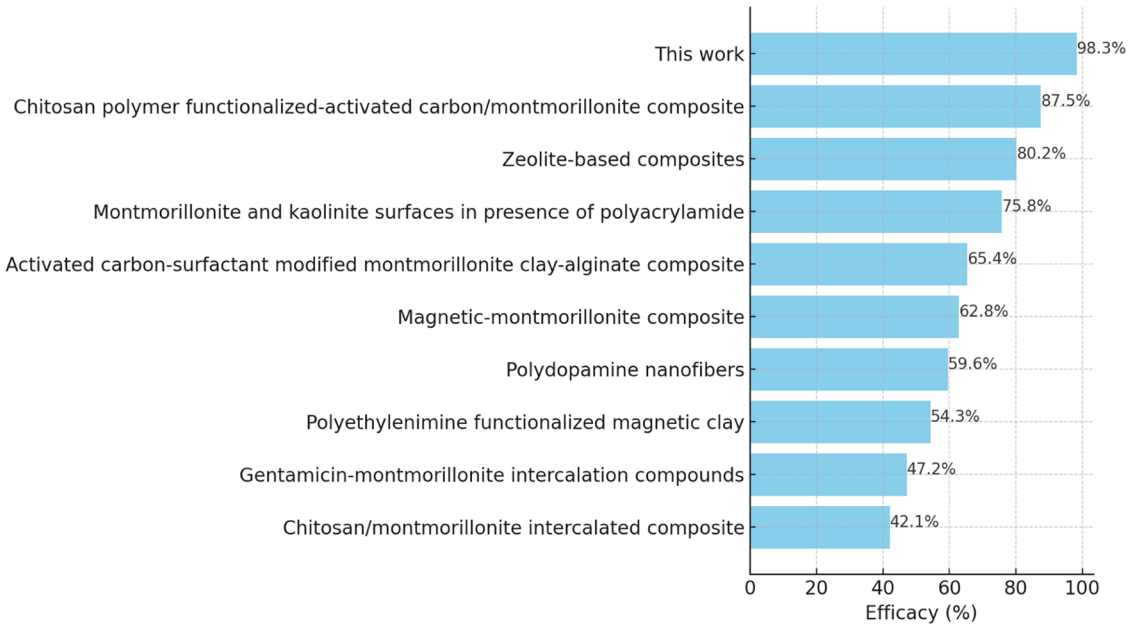

Figure 9. Comparison between the different adsorbent systems in the literature and PF-MMT.

- PF-MMT surface and functional groups: The surface of PF-MMT is covered with various functional groups like hydroxyl (−OH), carbonyl (C═O), and aromatic rings. These groups provide specific spots where lead ions can attach themselves.
- Ion exchange with clay: Inside PF-MMT, montmorillonite clay contains layers containing cations like Na^+, K^+, and Ca^{2+}. When lead ions come into contact with this clay, they swap places with these cations. This process is called ion exchange and helps in capturing lead ions.
- Coordination complexes formation: The oxygen-containing groups (like hydroxyl and carbonyl) on PF-MMT can grab and hold lead ions, forming stable structures known as coordination complexes.
- $\pi-\pi$ stacking interactions: The aromatic rings (ring-shaped molecules) in PF-MMT can interact with lead ions through a special type of attraction known as $\pi-\pi$ stacking, further helping in trapping these ions.
- Physical entrapment: PF-MMT has a porous structure with tiny spaces and channels. Lead ions can get physically trapped inside these spaces, much like small particles in a sponge.
- Electrostatic interactions: Lastly, the surface of PF-MMT is negatively charged, while lead ions are positively charged. Opposite charges attract, which helps pull lead ions out of the water and onto the PF-MMT surface.

In summary, PF-MMT uses a combination of chemical attractions and physical trapping to effectively remove lead ions from water, making it an efficient adsorbent.

3.7. Comparison with Previous Studies: Enhancing Lead Ion Adsorption from Aqueous Solution. Over the years, significant advancements have been made in adsorbent systems for removal of lead ions from aqueous solutions. Figure 9 comprehensively compares various materials used for this purpose, highlighting their efficacy percentages.

- This work (98.3% efficacy): The most recent development, labeled "this work," shows a remarkable efficacy of 98.3%. This indicates a significant improvement over previously studied materials, positioning it as the most effective option currently known for lead ion adsorption.
- Chitosan polymer functionalized-activated carbon/montmorillonite composite (87.5%): Previously, the chitosan polymer functionalized-activated carbon/montmorillonite composite was one of the top performers with an efficacy of 87.5%.[37]
- Other notable materials: The chart also includes materials like zeolite-based composites (80.2%),[38] montmorillonite and kaolinite surfaces with polyacrylamide (75.8%),[39] activated carbon-surfactant-modified montmorillonite clay-alginate composite (65.4%),[40] and magnetic-montmorillonite composite (62.8%).[41] Each of these has shown commendable efficacy in lead ion adsorption, yet they fall short compared to the recent developments.
- Continued innovation: The advancements from materials like polydopamine nanofibers,[42] polyethylenimine functionalized magnetic clay,[19] gentamicin-montmorillonite intercalation compounds,[43] and chitosan/montmorillonite intercalated composite[44−45464748] demonstrate the ongoing innovation in this field. They contribute valuable insights into material properties and interactions in adsorption processes despite lower efficacy rates.

4. CONCLUSIONS

The PF-MMT composite, derived from montmorillonite clay (MMT) and phenol formaldehyde resin (PF), was synthesized to create a resin (PF-MMT) with an exceptional capacity for efficiently removing Pb^{2+} from synthetic water. Experimental data fitting revealed that the pseudo-second-order kinetic model best represents the adsorption process, suggesting chemisorption or ion exchange mechanisms. The significant removal efficiency of the Pb^{2+} ions reached 98.33% at 90 min. Furthermore, the Langmuir isotherm model demonstrated a favorable adsorption process with a high affinity between the adsorbent and Pb^{2+}, resulting in a maximum adsorption capacity of 243.9 mg/g for PF-MMT. Thermodynamic analysis indicated an endothermic and spontaneous adsorption process, enhancing its suitability for water treatment. The DKR model supported

https://doi.org/10.1021/acsomega.3c09830
ACS Omega 2024, 9, 12015−12026

the chemical nature of the adsorption process, with an *E*-value of 14.85 kJ/mol. FTIR, SEM, and XRD characterizations of the functional groups and surface properties conducive to Pb^{2+} ion adsorption. In conclusion, these comprehensive findings underscore the potential of PF-MMT as a highly effective adsorbent for removing Pb^{2+} ions from an aqueous solution, emphasizing its significance for environmental remediation.

AUTHOR INFORMATION

Corresponding Author

Moaz M. Abdou − *Egyptian Petroleum Research Institute, Cairo 11727, Egypt*; orcid.org/0000-0003-0253-5714; Email: moaz.chem@gmail.com

Authors

Abdel-Ghany A. Soliman − *National Institute of Oceanography and Fisheries, Cairo 11796, Egypt*

Atef S. Kobisy − *Egyptian Petroleum Research Institute, Cairo 11727, Egypt*

Ahmed Abu-Rayyan − *Faculty of Science, Applied Science Private University, Amman 11931, Jordan*

Mohammad Al-Omari − *Faculty of Science, Applied Science Private University, Amman 11931, Jordan*

Hussah A. Alshwyeh − *Department of Biology, College of Science, Imam Abdulrahman Bin Faisal University, Dammam 31441, Saudi Arabia; Basic & Applied Scientific Research Center (BASRC), Imam Abdulrahman Bin Faisal University, Dammam 31441, Saudi Arabia*

Ahmed H. Ragab − *Chemistry Department, College of Science, King Khalid University, Abha 61413, Saudi Arabia*

Hossa F. Al Shareef − *Department of Chemistry, College of Applied Sciences, Umm Al-Qura University, Makkah 21955, Saudi Arabia*

Nabila S. Ammar − *Water Pollution Research Department, National Research Centre, Giza 12622, Egypt*

Complete contact information is available at: https://pubs.acs.org/10.1021/acsomega.3c09830

Notes

The authors declare no competing financial interest.

ACKNOWLEDGMENTS

The authors thank the Deanship of Scientific Research at King Khalid University for funding this work through a large group Research Project under grant number RGP 2/38/44.

DEDICATION

This work is dedicated to the memory of the pure soul of Professor Mohamed Abbas El-Metwally (D.Sc.), who was working at the Department of Chemistry, Faculty of Science, Mansoura University, Egypt.

REFERENCES

(1) Law, K. S.; Stohl, A. Arctic Air Pollution: Origins and Impacts. *Science* **2007**, *315* (5818), 1537−1540.

(2) Demirbas, A. Heavy Metal Adsorption onto Agro-Based Waste Materials: A Review. *J. Hazard. Mater.* **2008**, *157* (2−3), 220−229.

(3) Chowdhary, P.; Bharagava, R. N.; Mishra, S.; Khan, N. *Role of Industries in Water Scarcity and Its Adverse Effects on Environment and Human Health*; Springer eBooks, 2019; pp 235−256. DOI: 10.1007/978-981-13-5889-0_12.

(4) Dolati, S.; Ramezani, M.; Abnous, K.; Taghdisi, S. M. Recent Nucleic Acid Based Biosensors for Pb^{2+} Detection. *Sens. Actuators, B* **2017**, *246*, 864−878.

(5) Kulpa, A.; Ryl, J.; Schroeder, G.; Koterwa, A.; Anand, J. S.; Ossowski, T.; Niedziałkowski, P. Simultaneous Voltammetric Determination of Cd^{2+}, Pb^{2+}, and Cu^{2+} Ions Captured by Fe_3O_4@SiO_2 Core-Shell Nanostructures of Various Outer Amino Chain Length. *J. Mol. Liq.* **2020**, *314*, No. 113677.

(6) Aragay, G.; Pons, J.; Merkoçi, A. Recent Trends in Macro-, Micro-, and Nanomaterial-Based Tools and Strategies for Heavy-Metal Detection. *Chem. Rev.* **2011**, *111* (5), 3433−3458.

(7) Islam, M. R.; Gupta, S. S.; Jana, S. K.; Pradeep, T. Industrial Utilization of Capacitive Deionization Technology for the Removal of Fluoride and Toxic Metal Ions (As 3+/5+ and Pb^{2+}). *Global Challenges* **2022**, *6* (4), No. 2100129.

(8) Al-Saidi, H. M. Recent Advancements in Organic Chemosensors for the Detection of Pb^{2+}: A Review. *Chem. Pap.* **2023**, *77*, 4807.

(9) Chowdhury, I. R.; Chowdhury, S.; Mazumder, M. a. J.; Al-Ahmed, A. Removal of Lead Ions (Pb^{2+}) from Water and Aqueous solution: A Review on the Low-Cost Adsorbents. *Appl. Water Sci.* **2022**, *12* (8), No. 185, DOI: 10.1007/s13201-022-01703-6.

(10) Arsenie, T.; Cara, I. G.; Popescu, M.-C.; Motrescu, I.; Bulgariu, L. Evaluation of the Adsorptive Performances of Rapeseed Waste in the Removal of Toxic Metal Ions in Aqueous Media. *Water* **2022**, *14* (24), 4108.

(11) Ortiz-Oliveros, H. B.; Ouerfelli, N.; Cruz-González, D.; Ávila-Pérez, P.; Bulgariu, L.; Flaifel, M. H.; Abouzeid, F. M. Modeling of the Relationship between the Thermodynamic Parameters ΔH° and ΔS° with Temperature in the Removal of Pb Ions in Aqueous Medium: Case Study. *Chem. Phys. Lett.* **2023**, *814*, No. 140329.

(12) Ijagbemi, C. O.; Baek, M. H.; Kim, D. S. Montmorillonite Surface Properties and Sorption Characteristics for Heavy Metal Removal from Aqueous Solutions. *J. Hazard. Mater.* **2009**, *166* (1), 538−546.

(13) Bhattacharyya, K. G.; Gupta, S. Adsorption of a Few Heavy Metals on Natural and Modified Kaolinite and Montmorillonite: A Review. *Adv. Colloid Interface Sci.* **2008**, *140* (2), 114−131.

(14) Sen Gupta, S.; Bhattacharyya, K. G. Adsorption of Heavy Metals on Kaolinite and Montmorillonite: A Review. *Phys. Chem. Chem. Phys.* **2012**, *14* (19), 6698.

(15) Buruga, K.; Song, H.; Shang, J.; Bolan, N.; Kalathi, J. T.; Kim, K. A Review on Functional Polymer-Clay Based Nanocomposite Membranes for Treatment of Water. *J. Hazard. Mater.* **2019**, *379*, No. 120584.

(16) Zango, Z. U.; Garba, A.; Garba, Z. N.; Zango, M. U.; Usman, F.; Lim, J. W. Montmorillonite for Adsorption and Catalytic Elimination of Pollutants from Aqueous solution: A State-of-the-Arts Review. *Sustainability* **2022**, *14* (24), 16441.

(17) Lan, J.; Wang, B.; Bo, C.; Gong, B.; Ou, J. Progress on Fabrication and Application of Activated Carbon Sphere in Recent Decade. *J. Ind. Eng. Chem.* **2023**, *120*, 47−72.

(18) Hu, Z.-X.; Hu, X.; Cheng, W.; Lu, W. Influence of Synthetic Conditions on the Performance of Melamine−Phenol−Formaldehyde Resin Microcapsules. *High Perform. Polym.* **2019**, *31* (2), 197−210.

(19) Fijałkowska, G.; Wiśniewska, M.; Szewczuk-Karpisz, K.; Jędruchniewicz, K.; Oleszczuk, P. Comparison of Lead(II) Ions Accumulation and Bioavailability on the Montmorillonite and Kaolinite Surfaces in the Presence of Polyacrylamide Soil Flocculant. *Chemosphere* **2021**, *276*, No. 130088.

(20) Nampitch, T.; Magaraphan, R. The Removal of Rubber Particles from Skim Rubber Latex by Batch Adsorption Technique Using Organoclay. *Adv. Mater. Res.* **2013**, *787*, 122−126.

(21) Qutubuddin, S.; Fu, X.; Tajuddin, Y. Synthesis of Polystyrene-Clay Nanocomposites via Emulsion Polymerization Using a Reactive Surfactant. *Polym. Bull.* **2002**, *48* (2), 143−149.

(22) Singla, P.; Mehta, R.; Upadhyay, S. N. Clay Modification by the Use of Organic Cations. *Green Sustainable Chem.* **2012**, *02* (01), 21−25.

(23) Si, Y.; Li, J.; Cui, B.; Tang, D.; Yang, L.; Murugadoss, V.; Maganti, S.; Huang, M.; Guo, Z. Janus Phenol−Formaldehyde Resin and Periodic Mesoporous Organic Silica Nanoadsorbent for the Removal of

Heavy Metal Ions and Organic Dyes from Polluted Water. *Adv. Compos. Hybrid Mater.* **2022**, *5* (2), 1180−1195.
(24) Kavitha, D.; Murugavel, S. C.; Thenmozhi, S. Flame Retarding Cardanol Based Novolac-Epoxy/Rice Husk Composites. *Mater. Chem. Phys.* **2021**, *263*, No. 124225.
(25) Zhang, Y.-Y.; He, Y.; Zhang, K.-N.; Chen, Y.-G.; Ye, W. Montmorillonite Alteration and Its Influence on Sr (II) Adsorption on GMZ Bentonite. *Environ. Earth Sci.* **2021**, *80* (24), No. 791, DOI: 10.1007/s12665-021-10093-y.
(26) Chu, Y.; Khan, M. A.; Xia, M.; Wang, F.; Lei, W. Methionine-Montmorillonite Composite—A Novel Material for Efficient Adsorption of Lead Ions. *Adv. Powder Technol.* **2020**, *31* (2), 708−717.
(27) Schiewer, S.; Patil, S. B. Pectin-Rich Fruit Wastes as Biosorbents for Heavy Metal Removal: Equilibrium and Kinetics. *Bioresour. Technol.* **2008**, *99* (6), 1896−1903.
(28) Şenol, Z. M.; Şimşek, S. Insights into Effective Adsorption of Lead Ions from Aqueous Solutions by Using Chitosan-Bentonite Composite Beads. *J. Polym. Environ.* **2022**, *30* (9), 3677−3687.
(29) Kamali, M.; Esmaeili, H.; Tamjidi, S. Synthesis of Zeolite Clay/Fe-Al Hydrotalcite Composite as a Reusable Adsorbent for Adsorption/Desorption of Cationic Dyes. *Arab. J. Sci. Eng.* **2022**, *47* (5), 6651−6665.
(30) Yang, J.; Shojaei, S.; Shojaei, S. Removal of Drug and Dye from Aqueous Solutions by Graphene Oxide: Adsorption Studies and Chemometrics Methods. *npj Clean Water* **2022**, *5* (1), No. 5, DOI: 10.1038/s41545-022-00148-3.
(31) El-Saeed, R. A.; Hosny, R.; Fathy, M.; Abdou, M. M.; Shoueir, K. R. An Innovative SiO2-Pyrazole Nanocomposite for Zn(II) and Cr(III) Ions Effective Adsorption and Anti-Sulfate-Reducing Bacteria from the Produced Oilfield Water. *Arab. J. Chem.* **2022**, *15* (8), No. 103949.
(32) Rakhym, A. B.; Seilkhanova, G. A.; Kurmanbayeva, T. S. Adsorption of Lead (II) Ions from Water Solutions with Natural Zeolite and Chamotte Clay. *Mater. Today: Proc.* **2020**, *31*, 482−485.
(33) Djebbar, M.; Djafri, F.; Bouchekara, M.; Djafri, A. Adsorption of Phenol on Natural Clay. *Appl. Water Sci.* **2012**, *2* (2), 77−86.
(34) Jain, H.; Yadav, V.; Rajput, V. D.; Minkina, T.; Agarwal, S.; Garg, M. An Eco-Sustainable Green Approach for Biosorption of Methylene Blue Dye from Textile Industry Aqueous solution by Sugarcane Bagasse, Peanut Hull, and Orange Peel: A Comparative Study Through Response Surface Methodology, Isotherms, Kinetic, and Thermodynamics. *Water, Air, Soil Pollut.* **2022**, *233* (6), No. 187, DOI: 10.1007/s11270-022-05655-0.
(35) Jalees, M. I.; Farooq, M.; Basheer, S.; Asghar, S. Removal of Heavy Metals from Drinking Water Using Chikni Mitti (Kaolinite): Isotherm and Kinetics. *Arab. J. Sci. Eng.* **2019**, *44* (7), 6351−6359.
(36) Yahya, M. D.; Obayomi, K. S.; Abdulkadir, M. B.; Iyaka, Y. A.; Olugbenga, A. G. Characterization of Cobalt Ferrite-Supported Activated Carbon for Removal of Chromium and Lead Ions from Tannery Aqueous solution via Adsorption Equilibrium. *Water Sci. Eng.* **2020**, *13* (3), 202−213.
(37) Alexander, J. A.; Zaini, M. A. A.; Abdulsalam, S.; El-Nafaty, U. A.; Aroke, U. O. Isotherm Studies of Lead(II), Manganese(II), and Cadmium(II) Adsorption by Nigerian Bentonite Clay in Single and Multimetal Solutions. *Part. Sci. Technol.* **2019**, *37* (4), 403−413.
(38) Sharma, M.; Chouksey, S.; Gond, L.; Bajpai, A. A Hybrid Bionanocomposite for Pb (II) Ion Removal from Water: Synthesis, Characterization and Adsorption Kinetics Studies. *Polym. Bull.* **2022**, *79* (12), 10675−10706.
(39) Helfferich, F. Ion-exchange kinetics.1 III. experimental test of the theory of particle-diffusion controlled ion exchange. *J. Phys. Chem. A* **1962**, *66* (1), 39−44.
(40) Kumar, N.; Fosso-Kankeu, E.; Ray, S. S. Achieving Controllable MoS2 Nanostructures with Increased Interlayer Spacing for Efficient Removal of Pb (II) from Aquatic Systems. *ACS Appl. Mater. Interfaces* **2019**, *11* (21), 19141−19155.
(41) Alsohaimi, I. H.; Alhumaimess, M. S.; Hassan, H. M. A.; Reda, M.; Aldawsari, A. M.; Chen, Q.; Kariri, M. A. Chitosan Polymer Functionalized-Activated Carbon/Montmorillonite Composite for the Potential Removal of Lead Ions from Aqueous solution. *Polymers* **2023**, *15* (9), 2188.
(42) Rad, L. R.; Anbia, M. Zeolite-Based Composites for the Adsorption of Toxic Matters from Water: A Review. *J. Environ. Chem. Eng.* **2021**, *9* (5), No. 106088.
(43) Ullah, N.; Ali, Z.; Ullah, S.; Khan, A.; Adalat, B.; Nasrullah, A.; Alsaadi, M.; Ahmad, Z. Synthesis of Activated Carbon-Surfactant Modified Montmorillonite Clay-Alginate Composite Membrane for Methylene Blue Adsorption. *Chemosphere* **2022**, *309*, No. 136623.
(44) Fatimah, I.; Citradewi, P. W.; Fadillah, G.; Sahroni, I.; Purwiandono, G.; Dong, R.-A. Enhanced Performance of Magnetic Montmorillonite Nanocomposite as Adsorbent for Cu(II) by Hydrothermal Synthesis. *J. Environ. Chem. Eng.* **2021**, *9* (1), No. 104968.
(45) Jian, N.; Dai, Y.; Wang, Y.; Qi, F.; Li, S.; Wu, Y. Preparation of Polydopamine Nanofibers Mat as a Recyclable and Efficient Adsorbent for Simultaneous Adsorption of Multiple Tetracyclines in Water. *J. Cleaner Prod.* **2021**, *320*, No. 128875.
(46) Fayazi, M.; Ghanbarian, M. One-Pot Hydrothermal Synthesis of Polyethylenimine Functionalized Magnetic Clay for Efficient Removal of Noxious Cr(VI) from Aqueous Solutions. *Silicon* **2020**, *12* (1), 125−134.
(47) Darder, M.; He, J.; Charlet, L.; Ruiz-Hitzky, E.; Aranda, P. Gentamicin-Montmorillonite Intercalation Compounds as an Active Component of Hydroxypropylmethylcellulose Bionanocomposite Films with Antimicrobial Properties. *Clays Clay Miner.* **2021**, *69* (5), 576−588.
(48) Li, J.; Cai, J.; Zhong, L.; Cheng, H.; Wang, H.; Ma, Q. Adsorption of Reactive Red 136 onto Chitosan/Montmorillonite Intercalated Composite from Aqueous Solution. *Appl. Clay Sci.* **2019**, *167*, 9−22.

https://doi.org/10.1021/acsomega.3c09830
ACS Omega 2024, 9, 12015−12026